

No cataclysmic variables missing: higher merger rate brings into agreement observed and predicted space densities

Diogo Belloni^{1,2*}, Matthias R. Schreiber^{3,4†}, Mónica Zorotovic^{3‡},
 Krystian Iłkiewicz¹, Jarrod R. Hurley⁵, Mirek Giersz¹ and Felipe Lagos³

¹ Nicolaus Copernicus Astronomical Centre, Polish Academy of Sciences, ul. Bartycka 18, PL-00-716 Warsaw, Poland

² CAPES Foundation, Ministry of Education of Brazil, DF 70040-020, Brasília, Brazil

³ Instituto de Física y Astronomía, Universidad de Valparaíso, Av. Gran Bretaña 1111 Valparaíso, Chile

⁴ Millenium Nucleus for Planet Formation, Universidad de Valparaíso, Valparaíso 2360102, Chile

⁵ Centre for Astrophysics and Supercomputing, Swinburne University of Technology, Hawthorn, VIC 3122, Australia

Accepted 2018 May 29. Received 2018 May 4; in original form 2018 March 19

ABSTRACT

The predicted and observed space density of cataclysmic variables (CVs) have been for a long time discrepant by at least an order of magnitude. The standard model of CV evolution predicts that the vast majority of CVs should be period bouncers, whose space density has been recently measured to be $\rho \lesssim 2 \times 10^{-5} \text{ pc}^{-3}$. We performed population synthesis of CVs using an updated version of the Binary Stellar Evolution (BSE) code for single and binary star evolution. We find that the recently suggested empirical prescription of consequential angular momentum loss (CAML) brings into agreement predicted and observed space densities of CVs and period bouncers. To progress with our understanding of CV evolution it is crucial to understand the physical mechanism behind empirical CAML. Our changes to the BSE code are also provided in details, which will allow the community to accurately model mass transfer in interacting binaries in which degenerate objects accrete from low-mass main-sequence donor stars.

Key words: methods: numerical – novae, cataclysmic variables – stars: evolution.

1 INTRODUCTION

Cataclysmic variables (CVs) are interacting binaries composed of a white dwarf (WD) that accretes matter stably from a low-mass main-sequence (MS) or slightly evolved star (e.g. Knigge et al. 2011, for a comprehensive review). CVs are the most numerous close compact binary stars and are therefore superb systems to progress with our understanding of the long-term evolution of such systems. Despite successfully explaining crucial characteristics of the observed orbital period distribution of CVs, the standard model of CV evolution that has been developed during the last decades fails when confronted with other observations of CVs.

The most important feature observed in populations of CVs is the paucity of systems in the range of $2 \text{ hrs} \lesssim P_{\text{orb}} \lesssim 3 \text{ hrs}$, known as the *orbital period gap* (e.g. Knigge 2006). This orbital period gap is explained in the standard model for CV evolution by assuming disrupted magnetic braking (MB, Rappaport et al. 1982; Spruit & Ritter 1983; Howell et al. 2001). According to this scenario, a CV above the gap is driven towards shorter orbital periods

by angular momentum loss (AML) owing to gravitational radiation (GR) and MB. The latter is assumed to be orders of magnitudes stronger than the former at this stage and drives strong mass transfer. As a result of this strong mass transfer, the donor star is out of thermal equilibrium and significantly bloated compared to isolated MS stars of the same mass. When the donor star becomes fully convective (at an orbital period of $\approx 3 \text{ hrs}$), MB ceases, the mass transfer rate is reduced, and the donor star has time to relax to its thermal equilibrium radius. As a consequence, mass transfer completely stops and the CV converts into a close detached WD-MS binary until mass transfer starts again at an orbital period of $\approx 2 \text{ hrs}$. This explanation of the orbital period gap has been confirmed in several ways: Knigge (2006) showed that the radii of CVs at long orbital periods significantly exceed those of single MS stars; Schreiber et al. (2010) confirmed disrupted MB by showing that the evolutionary time-scale of post common envelope binaries (PCEBs) significantly increases at the fully convective boundary; and finally Zorotovic et al. (2016) provided the most direct evidence by identifying a population of detached CVs crossing the gap. Explaining successfully the existence of the orbital gap is a great achievement of the standard model for CV evolution.

The standard model also explains reasonably well the existence of a *minimum orbital period*, i.e. CVs do not appear to ex-

* E-mail: belloni@camk.edu.pl (DB)

† E-mail: matthias.schreiber@uv.cl (MRS)

‡ E-mail: mzorotovic@dfa.uv.cl (MZ)

ist with orbital periods shorter than a minimum value which is observationally determined to be at about 80 min (Gänsicke et al. 2009). In the context of the standard model, this can be explained as follows. After crossing the orbital period gap and restarting mass transfer again, the secondary is increasingly driven out of thermal equilibrium by mass loss. At some point, when the donor becomes strongly degenerate, its thermal time-scale exceeds the mass loss time-scale and as a consequence it expands in response to the mass loss which causes its orbital period to increase (e.g. King 1988). The CVs with substellar secondaries that have passed the orbital period minimum are called period bouncers and according to the standard model they should make up a large fraction of all CVs, e.g. Kolb (1993) predicted up to 70 per cent of all CVs should be period bouncers.

While the existence of a period gap and the period minimum are well explained by the standard scenario of CV evolution, other predictions of the model dramatically fail when compared to observations. The predicted space densities of CVs (e.g. de Kool 1992; Kolb 1993) exceed those derived from observations (e.g. Schreiber & Gänsicke 2003; Pretorius & Knigge 2012; Britt et al. 2015) by 1-2 orders of magnitude; models predict a larger fraction of systems residing below the gap than indicated by observations, and the WD masses expected in CVs are much smaller than those derived from observations (Zorotovic et al. 2011).

It is well-known that AML in CVs determines their secular evolution. Apart from the already mentioned systemic AML (i.e. MB and GR), which is independent of mass transfer, there is also AML that is a consequence of mass transfer. This type of AML does not act if there is no mass transfer and is therefore called *consequential* angular momentum loss (CAML, e.g. King & Kolb 1995). Candidates for CAML are circumbinary disks (e.g. Willems et al. 2005), hydromagnetic accretion disk winds (e.g. Cannizzo & Pudritz 1988), and AML associated with mass loss due to nova eruptions (King & Kolb 1995).

Recently, Schreiber et al. (2016) revised the standard model for CV evolution and showed that if CAML in CVs is inversely proportional to the WD mass, especially CVs with low-mass WDs run into dynamically unstable mass transfer and the WD and its companion merge. This can solve all three problems mentioned above (space density, WD mass, period distribution). In addition it seems that the merging CVs can explain the existence of single low-mass WDs (Zorotovic & Schreiber 2017). Despite some previously suggested formation scenarios for these single low-mass WDs, e.g. (i) single star evolution with enhanced mass loss (Castellani & Castellani 1993); (ii) mass ejection by massive planets (e.g. Nelemans & Tauris 1998); (iii) supernova stripping (e.g. Justham et al. 2009); or (iv) double helium-core WD merger (e.g. Saio & Jeffery 2000), the idea of producing the single low-mass WDs from merging CVs is attractive as the predicted relative numbers seem to perfectly match the observations (Zorotovic & Schreiber 2017).

The main mechanism thought to be responsible for the postulated dependence of CAML on WD mass are nova eruptions (Schreiber et al. 2016; Nelemans et al. 2016). Frictional AML produced by novae depends strongly on the expansion velocity of the ejecta (Schenker et al. 1998), and for low-mass WDs, the expansion velocity is small (Yaron et al. 2005). This may lead to strong AML by friction that makes most CVs with He WDs dynamically unstable and the two stars merge instead of experiencing stable mass transfer. However, as the details of the physical mechanism behind the proposed CAML prescription are not fully understood, this model is usually called empirical CAML (eCAML).

Here we further compare the predictions of this revised empirical model for CV evolution with observations. While Schreiber et al. (2016) only compared the relative numbers of CVs predicted by the classical and empirical CAML models, we here determine the space density of CVs by calibrating the relative values using the space density of single WDs. In particular, we also predict the space density of CVs with substellar donor stars for both models. Recently, Hernández Santisteban et al. (2018) estimated the space density of period bouncers by searching in the Sloan Digital Sky Survey (SDSS) Stripe 82 data for drop-out eclipses in a sample of more than 2000 apparently single WDs and found no such eclipses. This allowed them to infer an upper limit for the period bouncer space density of $\lesssim 2 \times 10^{-5} \text{ pc}^{-3}$.

We find that the predicted space densities are in agreement with observations if we assume eCAML while the classical model predicts more CVs than observed.

2 BSE CODE

The Binary Stellar Evolution (BSE) code developed by Hurley et al. (2000, 2002) is among the most frequently used codes to investigate secular evolution of CVs. It consists of a set of algorithms describing single and binary star evolution. The main advantage of BSE is its speed and the generally high level of accuracy in the analytic fitting formulae on which it is based.

Even though the BSE code is frequently used for population synthesis of CVs and related objects (e.g. Meng & Yang 2011; Zuo & Li 2011; Schreiber et al. 2016; Zorotovic & Schreiber 2017) it is best suited to modeling just the early phases of their evolution, i.e. from the zero-age MS until the formation of PCEBs (e.g. Schreiber et al. 2016; Zorotovic et al. 2016; Chen et al. 2014). This is mainly because the BSE code in its original form includes only a simple description of the evolution of accreting WD binary systems and comprehensive testing of degenerate mass-transfer phases was beyond the original scope. As such, fundamental ingredients of CV evolution are currently missing (Belloni et al. 2017, see Section 5.2), and using BSE for CVs can thus lead to inaccurate predictions for e.g. mass transfer rates, duty cycles, or the orbital period and donor star mass distributions of CVs.

To overcome these shortcomings of the original BSE code, we updated the code in order to include state-of-the-art prescriptions for CV evolution. Our new version allows accurate modeling of interacting binaries in which degenerate objects are accreting from low-mass MS donor stars. In particular, this revised BSE code is suitable for performing state-of-the-art simulations of CV evolution while it remains fast enough to allow for large population synthesis.

In what follows we briefly discuss the major changes, and provide more details in the Appendix. The main upgrade of the code is a revision of the mass transfer rate equation which is now based on the model of Ritter (1988) and has been properly calibrated for CVs (Section A1). We have also added the radius increase/decrease of low-mass MS donors that is expected when mass transfer is turned on/off (Section A2), which is fundamental to reproducing the observed orbital period gap in CV populations. We have also incorporated new options for systemic and CAML (Section A3), which now includes the MB prescription of Rappaport et al. (1983) and CAML prescriptions described in Schreiber et al. (2016). Finally, we have adopted different stability criteria for dynamical and thermal mass transfer from MS donors (Section A4), which now depend on the adiabatic mass-radius exponent and the mass-radius ex-

ponent of the MS star and on the assumed CAML (Schreiber et al. 2016).

In Section A5, we compare the predictions of the original BSE code with those obtained with our upgraded version for the evolution of individual CVs, and show that our modifications lead to mass transfer rates as well as orbital periods and donor masses in much better agreement with the observations.

3 BINARY POPULATION MODEL

We performed binary population synthesis using an initial population of one million binary stars generated according to the following initial distributions: (i) The primary is obtained from the initial mass function (IMF) proposed by Kroupa et al. (1993) in the range $[0.08, 100] M_{\odot}$; (ii) The secondary is obtained assuming a uniform mass ratio distribution, where $M_2 \leq M_1$, and requesting that $M_2 \geq 0.07$; (iii) The semi-major axis follows a log-uniform distribution in the range $[10^{-0.5}, 10^{4.5}] R_{\odot}$. (iv) The eccentricity follows a thermal distribution in the range $[0, 1]$.

For the common-envelope phase (CEP), we assumed that only 25 per cent of the variation in the binary orbital energy contributes to the expulsion of the CE, and that the binding energy parameter is variable and properly calculated assuming no contributions of recombination energy for expelling the CE. This set of parameters is consistent with recent investigations that have concluded that WD-MS binaries experience strong orbital shrinkage during the CEP (e.g. Zorotovic et al. 2010; Toonen & Nelemans 2013; Camacho et al. 2014; Cojocaru et al. 2017). We furthermore assume that the number of CVs that evolve through a phase of thermal time-scale mass transfer before becoming CVs is negligible. This is most likely a reasonable assumption as observations indicate that only 10 – 15 per cent of all CVs form through this channel (Gänsicke et al. 2003a). However, it is important to stress that even our new version of the BSE code is unable to properly model thermal time-scale mass transfer in CVs. This would require another modification of the prescriptions for mass transfer which is beyond the scope of the present paper. A recent attempt can be found in Wijnen et al. (2015) who intended to model thermal time scale mass transfer phase with the `binary_c` code (e.g. Izzard et al. 2006), which is similar to BSE, and concluded that a revision of the mass transfer equation was required. The fact that the revised BSE code presented here is unable to properly model thermal time scale mass transfer is clearly a flaw of the new code which should be carefully considered when analysing the distributions produced by the code.

As shown in Schreiber et al. (2016), the simulated population of CVs is strongly affected by the critical mass ratio that is defining the limit between stable and unstable mass transfer. Apart from the intrinsic (often also called systemic) AML due to GR and MB, CAML, i.e. AML due to mass transfer and mass loss during the nova eruptions, is expected to play a key role in CV evolution (Schreiber et al. 2016; Zorotovic & Schreiber 2017). We test here two different models for CAML: the classic model for CAML (cCAML, King & Kolb 1995), and the empirical CAML (eCAML), formulated by Schreiber et al. (2016) that recently has shown to solve several problems between model predictions and observations of CVs. See Section A3.1 for additional details about both prescriptions.

As in Goliašch & Nelson (2015), we assumed that the IMF is constant in time and that the binary fraction is 50 per cent (consistent with the binary fraction of WD primary progenitors, see

Patience et al. 2002). In addition, we assumed a constant star formation rate (Weidner et al. 2004) during the lifetime of the Galactic disk, which is assumed here to be ≈ 10 Gyr old. This way, the birth time of each binary and single star in the simulations is chosen randomly, assuming a uniform distribution, and they are evolved from the birth time until 10 Gyr.

In order to compute the CV space density, we follow the procedure described in Goliašch & Nelson (2015, see their sections 2.2.3 and 2.2.4). As we simulate both single stars and binaries, we can normalize the results of our population synthesis such that the number of single WDs corresponds to a specific birthrate of WDs in the Galactic disk. We adopt a WD formation rate of 0.4 WD yr^{-1} , which gives a total number of 4×10^9 WDs in the disk. The total number of CVs was scaled the same way to obtain absolute numbers of systems that should be present in the Galactic disk. Finally, we compute the space density by assuming a Galactic volume of $5 \times 10^{11} \text{ pc}^3$ (e.g. Toonen et al. 2017).

4 RESULTS

We ran population models of CVs using two prescriptions for CAML and determined the predicted space densities for all CVs and for period bouncers. Table 1 exhibits the number and space density of present-day single WDs, CVs and period bouncers predicted by our simulations.

The numbers of single WDs formed in our simulations, for both cCAML and eCAML, are similar, although the number in eCAML is slightly larger than in cCAML due to the fact that the critical mass ratio for stable mass transfer defined by eCAML leads to a narrower stable region in the parameter space of CVs (Schreiber et al. 2016, see, e.g. figs. 1 and 2), while most CVs whose primaries are low-mass WDs merge, leading to more single WDs (Zorotovic & Schreiber 2017). The same effect significantly reduces the CV space densities predicted by eCAML ($\approx 2 \times 10^{-5} \text{ pc}^{-3}$) compared to the classical model ($\approx 9 \times 10^{-5} \text{ pc}^{-3}$). As a much larger number of systems suffer dynamical unstable mass transfer, less systems experience stable AML-driven mass transfer.

Inspecting Table 1 in more detail, we find that the reduction in space density due to the implementation of eCAML is smaller for period bouncers than for the entire CV population. Therefore, the space density of the total CV population is somewhat less reduced than in Schreiber et al. (2016) who ignored period bouncers with secondary masses below $0.05 M_{\odot}$. This different effect of eCAML on the space densities of the entire CV population and period bouncers is caused by the mass dependence of the additional AML in the eCAML scenario as illustrated in Fig. 1.

By postulating that systems with low-mass WDs preferentially merge due to unstable mass transfer (for a visualisation of this effect in the WD mass vs. mass ratio plane see fig. 1 of Zorotovic & Schreiber 2017), the WD mass distribution of CVs predicted by eCAML contains only relatively massive WDs and these must have had quite massive MS star progenitors (upper left panel). The intermediate-mass MS stars have short MS lifetimes and the CEP is on average reached earlier than in the case of the classical model (upper right). The shorter MS lifetimes for the CV primary progenitors in the eCAML model then translate into shorter times until a CV reaches the orbital minimum (lower right panel). The shorter CV formation times in eCAML finally imply that this model predicts a flatter age distribution of CVs than the classical model (bottom right panel). Consequently, the relative fraction of CVs that are period bouncers is even larger in the

Table 1. Number and space density of present-day single WDs, CVs and period bouncers in our simulations, according to both models of CAML assumed here. The number of single WDs corresponds to the total amount of single WDs formed in both single and binary evolution. The number of CVs refers to the total amount of all types of CVs, i.e. long-period, gap CVs, short-period and period bouncers. The numbers presented in columns labeled *Modelling* corresponds to the number obtained in our simulations, while those in the columns labeled *Absolute* are scaled with respect to the single WD birth rate. Finally, the space density (ρ) was computed based on the absolute numbers, assuming a Galactic volume of $5 \times 10^{11} \text{ pc}^3$.

CAML	Single WDs			CVs			Period bouncers		
	Modelling	Absolute	$\rho [\text{pc}^{-3}]$	Modelling	Absolute	$\rho [\text{pc}^{-3}]$	Modelling	Absolute	$\rho [\text{pc}^{-3}]$
classical	95525	4×10^9	8×10^{-3}	1068	4.472×10^7	8.9×10^{-5}	717	3.002×10^7	6.0×10^{-5}
empirical	95979	4×10^9	8×10^{-3}	237	0.988×10^7	2.0×10^{-5}	181	0.754×10^7	1.5×10^{-5}

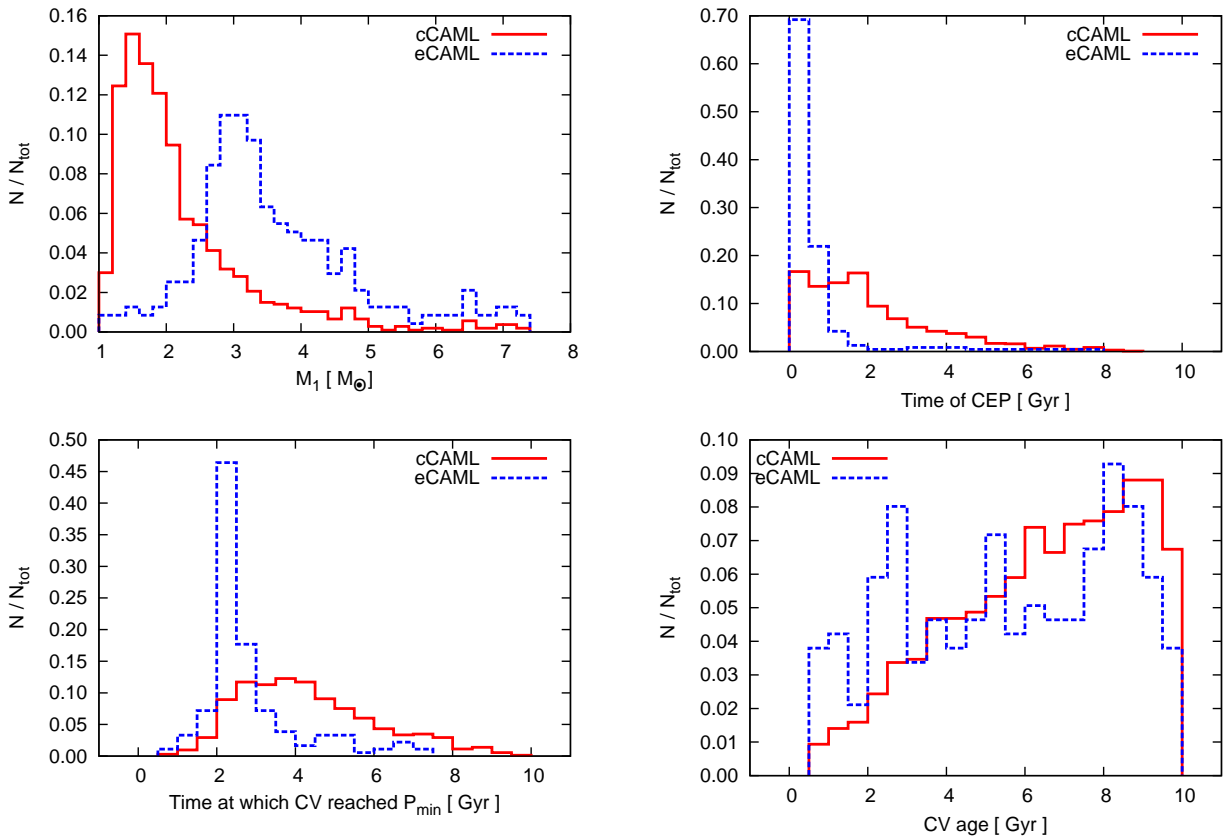


Figure 1. Distributions of all CVs in our simulations: WD progenitor mass (top left-hand panel), time at which the CEP takes place (top right-hand panel), time at which CVs reach the period minimum (bottom left-hand panel), and CV age (bottom right-hand panel).

eCAML model (76 per cent) than according to the standard theory (67 per cent)

The different evolutionary time-scales also affect the properties of the population of period bouncers as shown in Fig. 2. According to eCAML significantly more CVs have passed the period minimum more than ~ 5 Gyrs ago (top left-hand panel) and have therefore reached longer orbital periods (top right-hand panel) and lower secondary star masses (bottom left-hand panel). The WD mass distributions of the period bouncers (bottom right-hand panel) are similar to those of the entire CV population: while eCAML predicts only massive WD systems to become CVs, the distribution predicted by the classical model is dominated by low-mass WDs, which is inconsistent with observations.

One might think that the different evolutionary time scales

and the different WD masses predicted by the two models translate into a significant difference in the temperatures of the accreting WDs. In order to test if this is the case, we determined the effective temperature distributions of the predicted period bouncer populations by calculating both the cooling temperature of the WD and the temperature according to compressional heating. The former were determined as in Zorotovic & Schreiber (2017), i.e. via interpolation of DA (pure hydrogen atmosphere) WD evolutionary models by Althaus & Benvenuto (1997), for helium-core WDs, and by Fontaine et al. (2001), for carbon/oxygen-core WDs. The tem-

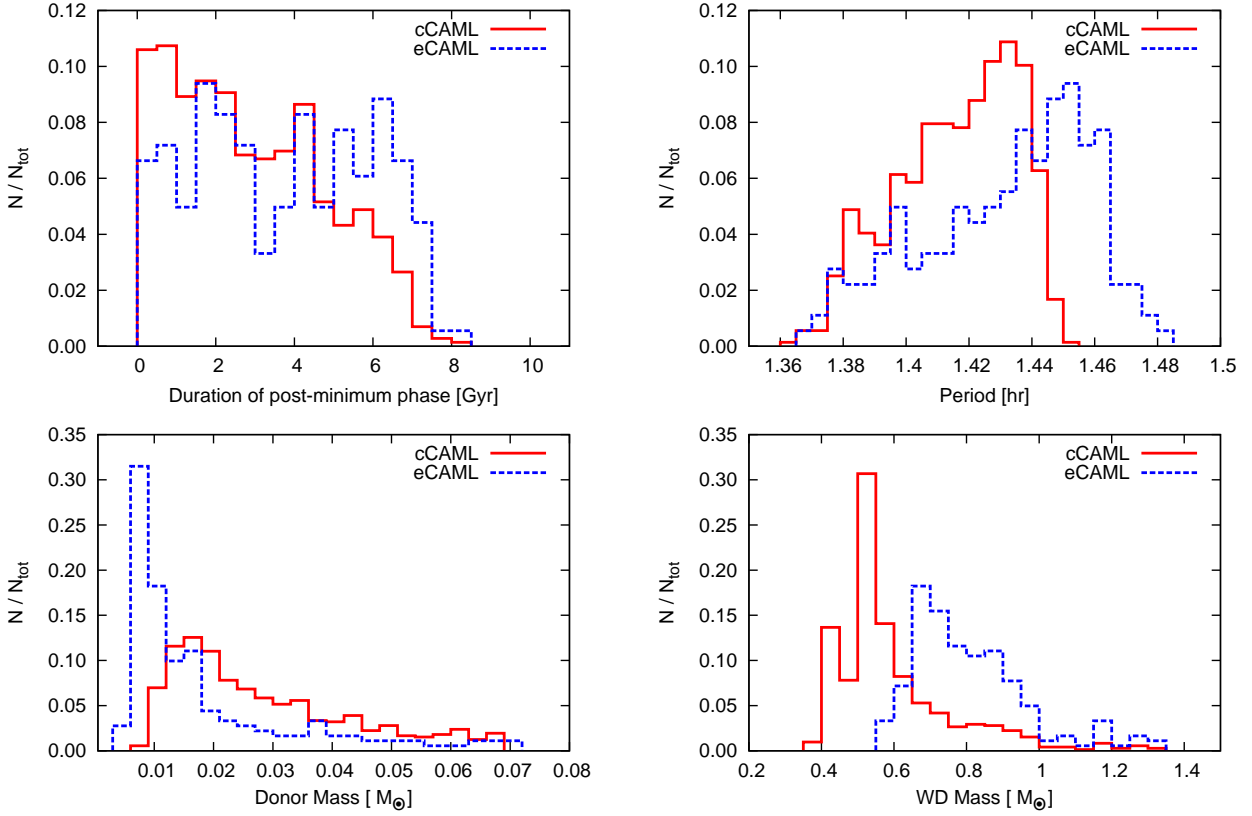


Figure 2. Distributions associated with period bouncers in our simulations: lifetime as period bouncers (top left-hand panel), orbital period (top right-hand panel), donor mass (bottom left-hand panel), and WD mass (bottom right-hand panel).

perature generated by compressional heating was determined from Eq. 2 in Townsley & Gänsicke (2009), i.e.

$$\frac{T_{\text{eff}}}{\text{K}} = 1.7 \times 10^4 \left(\frac{\langle \dot{M}_d \rangle}{10^{-10} M_{\odot} \text{ yr}^{-1}} \right)^{0.25} \left(\frac{M_{\text{WD}}}{0.9 M_{\odot}} \right), \quad (1)$$

where T_{eff} , $\langle \dot{M}_d \rangle$ and M_{WD} are the WD effective temperature due to compressional heating, the average mass transfer rate and the WD mass, respectively.

We find that in most cases, the compressional heating temperature exceeds the cooling temperature and therefore, based on Eq. 1, the mass transfer rate and the WD mass determine the WD effective temperature of most WDs in period bouncers. The resulting distributions are shown in Fig. 3. Apparently, both distributions are very similar. We find that this is because the effects of the higher WD masses and the larger ages (and therefore smaller mass transfer rates) predicted by eCAML cancel out each other: according to Eq. 1 higher WD masses lead to higher WD effective temperatures while the smaller accretion rates in systems that passed the period minimum long time ago cause the compressional heating temperature to decrease. For both models we therefore find that the predicted population of period bouncers is dominated by systems containing very cool WDs (~ 5000 K) which implies that the majority of these systems are very hard to find.

5 DISCUSSION

We performed binary population synthesis of CVs and calculated the space densities of CVs and period bouncers according to the standard model of CV evolution and the new empirical CAML model suggested by Schreiber et al. (2016).

Our simulations involve several model assumptions, such as a small CEP efficiency, flat initial mass ratio distribution, log-uniform semi-major axis distribution and constant star formation rate. Evidence is growing towards a low CEP efficiency (e.g. Zorotovic et al. 2010; Toonen & Nelemans 2013; Camacho et al. 2014; Cojocaru et al. 2017) and constant star formation rate (e.g. Kroupa et al. 2013; Recchi & Kroupa 2015; Schulz et al. 2015) but the situation with respect to initial binary distributions is less clear.

There seem to exist correlations amongst orbital parameters for different stellar spectral types (e.g. Duquennoy & Mayor 1991; Moe & Di Stefano 2017) and assuming uncorrelated distributions as done here might not be realistic. In the particular case of WD progenitors, De Rosa et al. (2014), by combining adaptive optics imaging and a multi-epoch common proper motion search, found for A-type stars that the semi-major axis distribution forms a log-normal distribution and the mass ratio distribution of closer ($a < 125$ AU) binaries is distinct from that of wider systems, with a flat distribution for close systems and a distribution that tends towards smaller mass ratios for wider binaries. Furthermore, Moe & Di Stefano (2017) investigated binaries whose primaries are mainly A, B and O-type stars, and after combining the samples from various surveys and correcting for their respec-

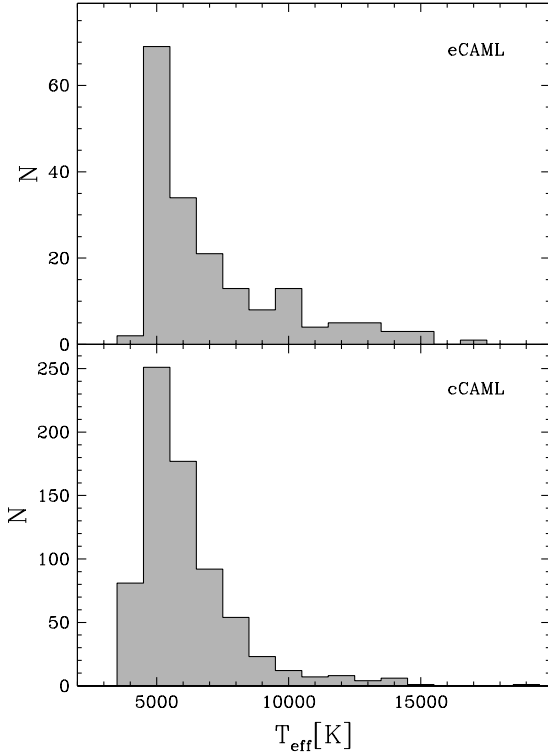


Figure 3. The predicted distribution of WD temperatures in period bouncers computed by comparing the cooling temperature of the WD and the temperature derived from compressional heating and selecting the higher value for each WD. Most WD temperatures, in both models, lie between 4000 and 7000 K.

tive selection effects, these authors concluded that the distributions are not independent and fitted joint probability density functions $f(M_1, q, P, e) \neq f(M_1)f(q)f(P)f(e)$ to the corrected distributions. These fitted joint distributions are probably the most realistic available to the community and should be incorporated into future binary population synthesis studies. In this paper we present the impact of different CAML prescriptions on the predicted space densities and therefore preferred to assume uncorrelated distributions for comparison with previous works. However, we plan to investigate the impact of more complex initial distributions on the results of binary population models in a future paper.

The values we obtain for the space density of CVs by assuming cCAML and eCAML are $\approx 0.9 \times 10^{-4} \text{ pc}^{-3}$ and $\approx 2 \times 10^{-5} \text{ pc}^{-3}$, respectively, i.e. the CV space density predicted by the eCAML model is considerably smaller than the value predicted by the classical model because a large number of systems merge instead of becoming CVs.

Previous theoretical estimates of the CV space density cluster around mid-plane space densities of 10^{-4} pc^{-3} and are thus in general agreement with the value we found assuming cCAML. Using the CV formation rate derived by *de Kool (1992)*, assuming an age of the Galaxy of 10 Gyrs and assuming that the lifetimes of CVs exceed this value, the predicted space density is $(0.5 - 2) \times 10^{-4} \text{ pc}^{-3}$. Normalizing the results of the binary population model for CVs from *Kolb (1993)* with the formation rate of single WDs, the predicted mid-plane CV space density is $1.8 \times 10^{-4} \text{ pc}^{-3}$. In both studies the classical CAML prescription

has been assumed. A significantly smaller value has been recently predicted by *Goliash & Nelson (2015)* who found a space density of $1.0(\pm 0.5) \times 10^{-5} \text{ pc}^{-3}$. However, these authors did not describe which criterion has been used to separate stable and unstable mass transfer and which form of CAML has been assumed in their calculations. It is therefore impossible to understand the significant difference to other previous predictions.

The smaller space density we obtain assuming eCAML is in very good agreement with the space densities derived from observations. For example, using the ROSAT North Ecliptic Pole survey *Pretorius et al. (2007)* obtained a space density of the CV population of $1.1^{+2.3}_{-0.7} \times 10^{-5} \text{ pc}^{-3}$ and *Hertz et al. (1990)* derived $\approx (2 - 3) \times 10^{-5} \text{ pc}^{-3}$ using the Einstein Galactic Plane Survey. *Schreiber & Gänsicke (2003)* derived a lower limit of $\sim 10^{-5} \text{ pc}^{-3}$ using a relatively small sample of PCEBs, the progenitors of CVs, and estimating their evolutionary lifetimes. This lower limit, however, is based on the cCAML assumption and would become much smaller if eCAML applies as many of the considered PCEBs would merge when mass transfer starts instead of becoming CVs. More recently, *Britt et al. (2015)* derive a space density of long-period CVs of $5.6(\pm 3.9) \times 10^{-6} \text{ pc}^{-3}$ using data from American Association of Variable Star Observers. A more comprehensive review of observational estimates of the space density of CVs can be found in *Hernández Santisteban et al. (2018, their Fig. 8)*. As the values derived from observations cluster around $\sim 10^{-5} \text{ pc}^{-3}$, agreement with model predictions can be reached if eCAML is assumed while the classical models predict values significantly exceeding those derived from observations.

An additional test for the different model predictions is offered by a recent measurement of an upper limit for the space density of CVs that passed the period minimum (*Hernández Santisteban et al. 2018*). This derived upper limit is relatively uncertain as it depends significantly on the assumed characteristic WD temperature (*Hernández Santisteban et al. 2018, see their fig. 7*). However, according to our models, realistic characteristic WD temperatures should lie in the range of 4000 – 7000 K for both models (see Fig. 3). Together with the different characteristic WD masses ($0.6 M_{\odot}$ for cCAML and $0.8 M_{\odot}$ for eCAML) and using Fig. 7 of *Hernández Santisteban et al. (2018)* this translates into upper limits derived from observations of $\sim 1 - 10 \times 10^{-4} \text{ pc}^{-3}$ (eCAML) and $\sim 4 - 60 \times 10^{-5} \text{ pc}^{-3}$ (cCAML) for the space density of period bouncers.

The upper limit derived from observations is similar to the model predictions in the case of cCAML ($\approx 6 \times 10^{-5} \text{ pc}^{-3}$) while it largely exceeds the prediction in the case of eCAML ($\approx 1.5 \times 10^{-5} \text{ pc}^{-3}$). This means that the observational constraints on the space density of period bouncers currently available are not sufficient to distinguish between the two models. Deeper surveys and/or with shorter cadence are required to test models for CV evolution.

However, while we cannot exclude the classical model based on the upper limit for period bouncers alone, taking into account the measured and predicted space densities of the entire CV population, it currently seems that the predictions of the eCAML model agree significantly better with the observations. We therefore predict that future surveys of period bouncers may find less systems than expected from the classical model because according to eCAML there are less period bouncers and those that exist have relatively long periods, low-mass companions, small accretion rates, and massive WDs. All these factors make their discovery even more challenging than the population predicted by the classical model.

6 CONCLUSION

We carried out population synthesis of cataclysmic variables (CVs) and the population of period bouncers among them and predicted space densities for both populations. We considered two prescriptions of CAML, namely the classical non-conservative and the recently suggested empirical model. The latter is a good candidate to solve several problems related to CV evolution, like the missing low-mass WDs in CVs or the period distribution (see Schreiber et al. 2016, for more details), and may also provide an explanation for the existence of single He-core WDs (Zorotovic & Schreiber 2017).

We confirm here that the space densities of CVs and period bouncers predicted by eCAML agree significantly better with the space densities derived from observations than the classical CV evolution model. However, eCAML is a purely empirical model and as an important next step towards a global understanding of CV evolution we need to investigate the physical origin of the enhanced CAML for systems with low-mass WDs. As suggested by Schreiber et al. (2016) and Nelemans et al. (2016) this origin might be found by studying the impact of nova eruptions and possible frictional AML on the secular evolution of CVs.

ACKNOWLEDGEMENTS

DB was supported by the CAPES foundation, Brazilian Ministry of Education through the grant BEX 13514/13-0 and by the National Science Centre, Poland, through the grant UMO-2016/21/N/ST9/02938. MRS acknowledges financial support from FONDECYT grant number 1141269. MZ acknowledges support from CONICYT PAI (Concurso Nacional de Inserción en la Academia 2017, Folio 79170121) and CONICYT/FONDECYT (Programa de Iniciación, Folio 11170559) KI has been financed by the Polish Ministry of Science and Higher Education Diamond Grant Programme via grant 0136/DIA/2014/43. MG was partially supported by the National Science Centre, Poland, through the grant UMO-2016/23/B/ST9/02732.

REFERENCES

- Althaus L. G., Benvenuto O. G., 1997, *ApJ*, **477**, 313
- Belloni D., Zorotovic M., Schreiber M. R., Leigh N. W. C., Giersz M., Askar A., 2017, *MNRAS*, **468**, 2429
- Britt C. T., et al., 2015, *MNRAS*, **448**, 3455
- Camacho J., Torres S., García-Berro E., Zorotovic M., Schreiber M. R., Rebassa-Mansergas A., Nebot Gómez-Morán A., Gänsicke B. T., 2014, *A&A*, **566**, A86
- Cannizzo J. K., Pudritz R. E., 1988, *ApJ*, **327**, 840
- Castellani M., Castellani V., 1993, *ApJ*, **407**, 649
- Chen H.-L., Woods T. E., Yungelson L. R., Gilfanov M., Han Z., 2014, *MNRAS*, **445**, 1912
- Claeys J. S. W., Pols O. R., Izzard R. G., Vink J., Verbunt F. W. M., 2014, *A&A*, **563**, A83
- Cojocaru R., Rebassa-Mansergas A., Torres S., García-Berro E., 2017, *MNRAS*, **470**, 1442
- Davis P. J., Kolb U., Willems B., Gänsicke B. T., 2008, *MNRAS*, **389**, 1563
- De Rosa R. J., et al., 2014, *MNRAS*, **437**, 1216
- Duquennoy A., Mayor M., 1991, *A&A*, **248**, 485
- Fontaine G., Brassard P., Bergeron P., 2001, *PASP*, **113**, 409
- Gänsicke B. T., et al., 2003a, *ApJ*, **594**, 443
- Gänsicke B. T., et al., 2003b, *ApJ*, **594**, 443
- Gänsicke B. T., et al., 2009, *MNRAS*, **397**, 2170
- Goliasch J., Nelson L., 2015, *ApJ*, **809**, 80
- González Hernández J. I., Suárez-Andrés L., Rebolo R., Casares J., 2017, *MNRAS*, **465**, L15
- Gustafsson B., Edvardsson B., Eriksson K., Jørgensen U. G., Nordlund Å., Plez B., 2008, *A&A*, **486**, 951
- Hernández Santisteban J. V., Knigge C., Pretorius M. L., Sullivan M., Warner B., 2018, *MNRAS*, **473**, 3241
- Hertz P., Bailyn C. D., Grindlay J. E., García M. R., Cohn H., Lugger P. M., 1990, *ApJ*, **364**, 251
- Hjellming M. S., 1989, PhD thesis, Illinois Univ. at Urbana-Champaign, Savoy.
- Howell S. B., Nelson L. A., Rappaport S., 2001, *ApJ*, **550**, 897
- Hurley J. R., Pols O. R., Tout C. A., 2000, *MNRAS*, **315**, 543
- Hurley J. R., Tout C. A., Pols O. R., 2002, *MNRAS*, **329**, 897
- Izzard R. G., Dray L. M., Karakas A. I., Lugaro M., Tout C. A., 2006, *A&A*, **460**, 565
- Justham S., Wolf C., Podsiadlowski P., Han Z., 2009, *A&A*, **493**, 1081
- Kalomeni B., Nelson L., Rappaport S., Molnar M., Quintin J., Yakut K., 2016, *ApJ*, **833**, 83
- King A. R., 1988, *QJRAS*, **29**, 1
- King A. R., Kolb U., 1995, *ApJ*, **439**, 330
- Knigge C., 2006, *MNRAS*, **373**, 484
- Knigge C., Baraffe I., Patterson J., 2011, *ApJS*, **194**, 28
- Kolb U., 1993, *A&A*, **271**, 149
- Kroupa P., Tout C. A., Gilmore G., 1993, *MNRAS*, **262**, 545
- Kroupa P., Weidner C., Pflamm-Altenburg J., Thies I., Dabringhausen J., Marks M., Maschberger T., 2013, The Stellar and Sub-Stellar Initial Mass Function of Simple and Composite Populations. p. 115, doi:10.1007/978-94-007-5612-0_4
- Meng X.-C., Yang W.-M., 2011, *Research in Astronomy and Astrophysics*, **11**, 965
- Moe M., Di Stefano R., 2017, *ApJS*, **230**, 15
- Muñoz-Darias T., et al., 2016, *Nature*, **534**, 75
- Nelemans G., Tauris T. M., 1998, *A&A*, **335**, L85
- Nelemans G., Siess L., Repetto S., Toonen S., Phinney E. S., 2016, *ApJ*, **817**, 69
- Pala A. F., et al., 2017, *MNRAS*, **466**, 2855
- Parsons S. G., et al., 2015, *MNRAS*, **452**, 1754
- Patience J., Ghez A. M., Reid I. N., Matthews K., 2002, *AJ*, **123**, 1570
- Paxton B., Bildsten L., Dotter A., Herwig F., Lesaffre P., Timmes F., 2011, *ApJS*, **192**, 3
- Paxton B., et al., 2015, *ApJS*, **220**, 15
- Politano M., 1996, *ApJ*, **465**, 338
- Pretorius M. L., Knigge C., 2012, *MNRAS*, **419**, 1442
- Pretorius M. L., Knigge C., Kolb U., 2007, *MNRAS*, **374**, 1495
- Rappaport S., Joss P. C., Webbink R. F., 1982, *ApJ*, **254**, 616
- Rappaport S., Verbunt F., Joss P. C., 1983, *ApJ*, **275**, 713
- Recchi S., Kroupa P., 2015, *MNRAS*, **446**, 4168
- Ritter H., 1988, *A&A*, **202**, 93
- Saio H., Jeffery C. S., 2000, *MNRAS*, **313**, 671
- Schenker K., Kolb U., Ritter H., 1998, *MNRAS*, **297**, 633
- Schenker K., King A. R., Kolb U., Wynn G. A., Zhang Z., 2002, *MNRAS*, **337**, 1105
- Schreiber M. R., Gänsicke B. T., 2003, *A&A*, **406**, 305
- Schreiber M. R., et al., 2010, *A&A*, **513**, L7
- Schreiber M. R., Zorotovic M., Wijnen T. P. G., 2016, *MNRAS*, **455**, L16
- Schulz C., Pflamm-Altenburg J., Kroupa P., 2015, *A&A*, **582**, A93
- Spruit H. C., Ritter H., 1983, *A&A*, **124**, 267
- Stehle R., Kolb U., Ritter H., 1997, *A&A*, **320**, 136
- Toonen S., Nelemans G., 2013, *A&A*, **557**, A87
- Toonen S., Nelemans G., Portegies Zwart S., 2012, *A&A*, **546**, A70
- Toonen S., Hollands M., Gänsicke B. T., Boekholt T., 2017, *A&A*, **602**, A16
- Townsend D. M., Gänsicke B. T., 2009, *ApJ*, **693**, 1007
- Weidner C., Kroupa P., Larsen S. S., 2004, *MNRAS*, **350**, 1503
- Whyte C. A., Eggleton P. P., 1980, *MNRAS*, **190**, 801
- Wijnen T. P. G., Zorotovic M., Schreiber M. R., 2015, *A&A*, **577**, A143
- Willems B., Kolb U., Sandquist E. L., Taam R. E., Dubus G., 2005, *ApJ*, **635**, 1263
- Yaron O., Prialnik D., Shara M. M., Kovetz A., 2005, *ApJ*, **623**, 398

- Zorotovic M., Schreiber M. R., 2017, *MNRAS*, **466**, L63
 Zorotovic M., Schreiber M. R., Gänsicke B. T., Nebot Gómez-Morán A., 2010, *A&A*, **520**, A86
 Zorotovic M., Schreiber M. R., Gänsicke B. T., 2011, *A&A*, **536**, A42
 Zorotovic M., Schreiber M. R., Parsons S. G., 2014, *A&A*, **568**, L9
 Zorotovic M., et al., 2016, *MNRAS*, **457**, 3867
 Zuo Z.-Y., Li X.-D., 2011, *ApJ*, **733**, 5
 de Kool M., 1992, *A&A*, **261**, 188

This paper has been typeset from a $\text{\TeX}/\text{\LaTeX}$ file prepared by the author.

APPENDIX A: UPGRADES TO THE BSE CODE FOR POPULATION SYNTHESIS OF CVs

We describe here the main upgrades to the BSE code which include a new mass transfer rate equation when the donor is a Roche lobe underfilling star (Section A1), a new method for the response of low-mass MS donor stars to mass transfer (Section A2), new AML prescriptions (Section A3), and new instability criteria for thermal and dynamical time scale mass transfer (Section A4). The upgrades we applied to BSE bring CV evolution and observations into agreement.

A1 Mass transfer onto degenerate objects

In the original version of the BSE code, Hurley et al. (2002) modelled the mass transfer rate using an equation that depends on the fraction of the donor that is overfilling its Roche lobe ($R_d/R_{L,d}$), i.e.

$$\dot{M}_d = f(M_d) [\ln(R_d/R_{L,d})]^3 M_\odot \text{yr}^{-1}, \quad (\text{A1})$$

where R_d is the donor radius, $R_{L,d}$ is the donor Roche lobe radius, M_d is the donor mass, and the factor $f = 3 \times 10^{-6} [\min(M_d, 5.0)]^2$ comes from numerical experiments (see also Whyte & Eggleton 1980). Despite some recent improvements (e.g. Claeys et al. 2014; Wijnen et al. 2015), this prescription leads to inaccurate mass transfer rates if mass transfer is driven by AML such as in CVs and low-mass X-ray binaries. This is because Eq. A1 does not account for the structure of the donor star. In particular, it neglects the finite scale height of the donor's atmosphere. In order to provide a mass transfer equation that works for CVs and related objects, we follow Ritter (1988) who considered that stars have extended atmospheres such that Roche lobe overflow can occur even if $R_d < R_{L,d}$. In this case we use the following equation

$$\dot{M}_d = \dot{M}_0 \times \exp\left(-\frac{R_{L,d} - R_d}{H_P}\right) M_\odot \text{yr}^{-1}, \quad (\text{A2})$$

where \dot{M}_0 is the mass transfer rate when the donor fills exactly its Roche lobe and H_P is the pressure scale height at the donor's photosphere. The pressure scale height at the donor's photosphere is computed based on Eq. 8b in Ritter (1988), i.e.

$$H_P = \frac{\mathfrak{X} T_d R_{L,d}^2}{\mu G M_d}, \quad (\text{A3})$$

where T_d is the donor's effective temperature, \mathfrak{X} is the gas constant, μ is the mean molecular weight, and G is the gravitational constant. In addition, we calculate \dot{M}_0 according to

$$\dot{M}_0 = \frac{2\pi}{\sqrt{2.71828}} \left(\frac{\mathfrak{X} T_d}{\mu}\right)^{3/2} \frac{R_{L,d}^3}{G M_d} \rho_{ph} F(q), \quad (\text{A4})$$

where ρ_{ph} is the density in the donor's photosphere and $F(q) \simeq 1.23 + 0.4 \log q$ (see appendix of Ritter 1988), where $q = M_d/M_a$ is the mass ratio and M_a is the accretor mass. In order to calculate ρ_{ph} we employed MARCS model atmospheres (Gustafsson et al. 2008) and created a grid of densities at an optical depth of $2/3$ (ρ_{ph}) for different T_d , donor's surface gravities, and metallicities. The resulting grid was interpolated to obtain ρ_{ph} for a given donor star. In cases where the donor becomes strongly degenerate ($M_d \lesssim 0.085 M_\odot$) MARCS model atmospheres become inaccurate and we thus use $\dot{M}_0 = 6.4 \times 10^{-9} M_\odot \text{yr}^{-1}$ and $H_P = 10^{-4} R_d$ (Ritter

1988, table A1). Equation A2 has been largely used to calculate mass transfer rates of CVs (e.g. Davis et al. 2008; Knigge et al. 2011; Zorotovic et al. 2016) and accurately describes the physical processes occurring when mass transfer is turning on or off. In addition, mass transfer rates in CVs calculated according to Eq. A2 generally agree with those derived from observations (depending on the assumed magnetic braking prescription, of course).

According to equation A2 Roche-lobe overflow starts when the extended atmosphere of the secondary reaches the Roche-radius, i.e. when the ratio between photospheric radius and Roche-radius is still smaller than 1. As explained in detail in Davis et al. (2008), calculating proper mass transfer rates from Eq. A2 requires to use relatively small time steps ($\lesssim 10^{3-4}$ yrs) to keep the filling factor below 1.00001 as otherwise the mass transfer rates become unrealistically high. This makes the revised BSE code somewhat slower, as we will discuss in Section A6. Finally, we note that Eq. A2 is only applied in the upgraded code for binaries in which a degenerate object (WD, neutron star or black hole) is accreting from either MS or giant stars underfilling their Roche lobe. Otherwise, Eq. A1 is used to estimate the mass transfer rate.

A2 Donor expansion due to mass transfer from low-mass MS stars

With the new mass transfer algorithm, BSE reproduces the mass transfer rates predicted by other population models of CVs and those derived from observations of CVs. However, even with this new prescription for the mass transfer rates, BSE is not able to reproduce the most important feature in the observed orbital period distribution of CVs, i.e. the paucity of systems with orbital periods in the range of 2 – 3 hrs.

In order to simulate CV evolution with BSE we do not only need to upgrade the mass transfer algorithm as described in the previous section, we also need to incorporate the radius increase of low-mass MS donor stars as they respond to strong mass loss. The amount by which mass losing low-mass MS donors are bloated relative to an isolated star of the same mass depends on how much their thermal time-scale exceeds the mass loss time-scale. Knigge et al. (2011) derived radii of CV donors from observations of a relatively large sample of CVs and found CVs above the orbital period gap to be bloated by about 30 per cent. In the original BSE code, the donor stars are not inflated which results in incorrect evolutionary tracks for CVs. Most importantly, without the increased radii of donor stars above the gap, it is impossible to reproduce the orbital period gap in binary population synthesis calculations. We include this fundamental ingredient of CV evolution in the upgraded BSE code by following Wijnen et al. (2015), i.e. we increase the donor star radii as soon as mass transfer starts until it reaches the value derived from observations (Knigge et al. 2011).

More specifically, the procedure is as follows. Let us consider first CVs that are born above the gap ($M_d \geq 0.35 M_\odot$). For these we define a factor that regulates the inflation from the equilibrium radius to the CV donor star radius as

$$f_c = \frac{R_{d,CV}^{\text{above}}}{R_{d,eq}}, \quad (\text{A5})$$

where $R_{d,CV}^{\text{above}} = 0.293(M_d/0.2)^{0.69}$ (Knigge et al. 2011) is the CV donor radius above the gap and $R_{d,eq}$ is the equilibrium radius computed by BSE in the standard way. In order to have a smooth transition from the equilibrium radius to the inflated radius, we let the donor inflate exponentially with time, i.e.

$$R_d = R_{d,inf} = \left[f_c + (1 - f_c)e^{-t/10} \right] R_{d,eq}, \quad (\text{A6})$$

where t in units of Myr is the time since the donor started to lose mass. We assume that MB becomes inefficient when the donor mass reduces to $0.2 M_\odot$. This mass limit is significantly smaller than for single M dwarfs or M dwarfs in detached binaries ($0.3-0.35 M_\odot$) because the mass transfer above the gap drives the secondary out of thermal equilibrium (see e.g. Knigge 2006, for details). At this point, the donor has time to relax to its thermal equilibrium radius. This can be described using an exponential ansatz (see Appendix of King & Kolb 1995). We use the following prescription (see

also Davis et al. 2008):

$$R_d = \left[1 - (1 - f_{\max})e^{-t/10}\right] R_{d,\text{inf}}, \quad (\text{A7})$$

where t (in units of Myrs) is the time since the donor detached from its Roche lobe and $f_{\max} = R_d/R_{d,\text{CV}}^{\text{below}}$ is the maximum inflation factor with respect to the CV donor star radius below the gap, and $R_{d,\text{CV}}^{\text{below}} = 0.225(M_d/0.2)^{0.61}$ (Knigge et al. 2011). After the system has evolved as a detached binary through the gap, at an orbital period of ≈ 2 hrs, mass transfer starts again. We then again inflate the donor but to a lesser extent by using $R_{d,\text{CV}}^{\text{above}} = R_{d,\text{CV}}^{\text{below}}$ in Eq. A5. The same procedure, i.e. inflate the donor up to a radius given by $R_{d,\text{CV}}^{\text{below}}$, is applied for CVs that are born in or below the gap ($M_d < 0.35 M_\odot$). Finally, for period-bouncers ($M_d < 0.069 M_\odot$), we simply adopt $R_d = 0.118(M_d/0.069)^{0.3}$ (Knigge et al. 2011).

A3 Angular momentum loss

The original version of BSE contains a prescription for disrupted MB and takes into account AML through GR and tides (Hurley et al. 2002, Sections 2.2, 2.3, and 2.4, respectively). In our upgraded version all procedures related to AML due to stellar winds and tides remain the same as in the original version. However, in the new version we provide an alternative MB prescription and normalization factors for MB and GR particularly suitable for CV evolution. We also add the possibility for additional AML that is generated by mass transfer, usually called consequential angular momentum loss (CAML, \dot{J}_{CAML}) (e.g. King & Kolb 1995).

A3.1 Consequential angular momentum loss

A potentially important ingredient for describing the evolution of close compact binary stars, in particular for CVs, is CAML which can significantly enhance the systemic AML generated by MB and GR. It is clear that CAML exists in CVs as mass and also angular momentum is lost during nova eruptions. Recently, Schreiber et al. (2016) and Nelemans et al. (2016) also discussed the possibility of additional AML due to frictional drag forces following nova eruptions. Alternative mechanisms for CAML in CVs are circumbinary disks (e.g. Willems et al. 2005) or hydromagnetic accretion disk winds (e.g. Cannizzo & Pudritz 1988). In low-mass X-ray binaries drag forces similar to those suggested by Schreiber et al. (2016) and Nelemans et al. (2016) might operate following X-ray bursts (González Hernández et al. 2017) as observed in V404 Cygni (Muñoz-Darias et al. 2016).

We have included two formulations for CAML in the revised BSE code, namely the classical CAML (cCAML) from King & Kolb (1995) and the empirical formulation (eCAML) from Schreiber et al. (2016). In cCAML it is assumed that the material leaving the system during a nova eruption carries the specific angular momentum of the WD, while eCAML is purely empirical and assumes stronger CAML for low-mass WDs to explain the absence of CVs with low-mass WD primaries (Zorotovic et al. 2011). The corresponding formulae we incorporated in the BSE code are:

$$\frac{\dot{J}_{\text{CAML}}}{J} = \nu \frac{\dot{M}_d}{M_d}, \quad (\text{A8})$$

where

$$\nu = \begin{cases} \frac{M_d^2}{M_a(M_a + M_d)}, & \text{classical (King \& Kolb 1995)} \\ \frac{0.35}{M_a}, & \text{empirical (Schreiber et al. 2016)} \end{cases} \quad (\text{A9})$$

Both CAML prescriptions are optional in the upgraded BSE code and can be turned on/off if desired. However, if the user of BSE aims at simulating CV populations, assuming no CAML will likely lead to unrealistic results as mass and AML during nova eruptions will be overlooked.

A3.2 Magnetic braking (MB) and gravitational radiation (GR)

First of all, it is important to note that, in general, the strength and form of AML owing to MB is highly uncertain and we currently rely entirely on empirical relations. Systemic AML in the original BSE code is modeled as described in Hurley et al. (2002, Section 2.4, Eqs. 48 and 50). This relation for MB seems to underestimate \dot{J}_{MB} in CVs as the resulting accretion rates are significantly smaller than those derived from observations (Pala et al. 2017). Therefore, in the upgraded code, the equation for AML owing to MB was replaced with a prescription more commonly used to simulate CV evolution:

$$\dot{J}_{\text{MB}} = -5.83 \times 10^{-16} M (R\Omega_{\text{spin}})^3 M_\odot R_\odot^2 \text{yr}^{-2}, \quad (\text{A10})$$

where M and R are the star mass and radius, respectively, both in solar units, and Ω_{spin} is the star spin in units of year (Rappaport et al. 1983). Eq. A10 provides AML rates in better agreement with standard models of CV evolution and mass transfer rates similar to those derived from observations. In the upgraded version of BSE the equation for AML due to GR remains the same as in the original.

To reach agreement with the observations of CVs, it might be required to adopt normalization factors for both AML prescriptions which strongly depend on the assumed CAML. If the classical CAML (or none) is assumed, then the normalization factors for MB and GR are 0.66 and 2.47 (Knigge et al. 2011), respectively, and if the empirical CAML is adopted, they are 0.43 and 1.67 (Zorotovic et al. 2016), respectively. We emphasize that these normalization factors are needed in order to reconcile observed properties of CVs, such as mass transfer rates, as well as the location of the orbital period minimum. Whenever using the upgraded version of BSE one should thus keep in mind that these are purely empirical factors and that the physics behind them is far from understood.

A4 Stability of mass transfer

As explained by Schreiber et al. (2016), the stability of mass transfer can be translated into a critical mass-ratio $q_{\text{crit}} = M_d/M_a$ above which mass transfer is unstable (usually, dynamically or thermally). These authors also showed that q_{crit} strongly depends on the adopted form of CAML at the onset of mass transfer (see also King & Kolb 1995).

In the original BSE code, the critical mass ratio for mass transfer on a dynamical time-scale is fixed to $q_{\text{crit}}^{\text{dyn}} = 0.695$ for low-mass MS donors ($M \lesssim 0.8 M_\odot$), and no limit is applied for more massive MS stars (although $q_{\text{crit}}^{\text{dyn}} = 3$ was subsequently added to the code after publication). A more accurate way of determining $q_{\text{crit}}^{\text{dyn}}$ in CVs is to compare the adiabatic mass-radius exponent ζ_{ad} of the MS star and the mass-radius exponent of the MS star Roche lobe ζ_{RL} . Therefore, in the upgraded BSE code we replaced the old criterion with the following. For low-mass MS stars (i.e. $M_d \leq 0.8 M_\odot$), if $\zeta_{\text{RL}} > \zeta_{\text{ad}}$ then the CV is dynamically unstable, and stable otherwise. For more massive MS stars, $q_{\text{crit}}^{\text{dyn}} = 3.0$. Note that ζ_{RL} is given by Schreiber et al. (2016) as

$$\zeta_{\text{RL}} = \frac{2}{3} \left(\frac{\ln(1 + q^{1/3}) - \frac{1}{2} \frac{q^{1/3}}{1 + q^{1/3}}}{0.6q^{2/3} + \ln(1 + q^{1/3})} \right) + 2\nu + \frac{M_d}{M_a + M_d} - 2, \quad (\text{A11})$$

where ν is given by Eq. A9. Alternatively, if CAML is not adopted, then (Schreiber et al. 2016)

$$\zeta_{\text{RL}} = \frac{2}{3} \left(\frac{\ln(1 + q^{1/3}) - \frac{1}{2} \frac{q^{1/3}}{1 + q^{1/3}}}{0.6q^{2/3} + \ln(1 + q^{1/3})} \right) (1 + q) + 2(q - 1). \quad (\text{A12})$$

Finally, ζ_{ad} is given by

$$\zeta_{\text{ad}} = \begin{cases} -\frac{1}{3}, & \text{if } M_d \leq 0.38412 M_\odot, \\ f(M_d), & \text{if } 0.38412 < M_d/M_\odot \leq 0.8, \end{cases} \quad (\text{A13})$$

where $f(M_d) = 0.782 - 7.464M_d + 13.925M_d^2 - 5.389M_d^3$ (Hjellming

$$q_{\text{crit}}^{\text{th}} = \begin{cases} 10.0566M_d^2 - 4.54427M_d + 1.60779, & \text{if } M_d \leq 0.25, \\ -11.6147M_d^3 + 14.8259M_d^2 - 5.38702M_d + 1.69848, & \text{if } 0.25 < M_d \leq 0.58, \\ 23.9492M_d^3 - 50.3456M_d^2 + 34.3213M_d - 6.35018, & \text{if } 0.58 < M_d \leq 0.82, \\ -17.2016M_d^3 + 51.4274M_d^2 - 49.7704M_d + 16.8633, & \text{if } 0.82 < M_d \leq 1.17, \\ -2.01893M_d^5 - 10.5146M_d^4 + 109.538M_d^3 - 278.879M_d^2 + 289.253M_d - 106.499, & \text{if } 1.17 < M_d \leq 1.7, \\ 0.185428M_d^2 - 0.552334M_d + 1.35125, & \text{if } 1.7 < M_d \leq 2.0, \\ -0.123087M_d^2 + 0.63407M_d + 0.211319, & \text{if } 2.0 < M_d \leq 2.35, \\ 0.00982875M_d^3 - 0.105005M_d^2 + 0.378526M_d + 0.585724, & \text{if } M_d > 2.35. \end{cases} \quad (\text{A14})$$

1989). Similarly, we define a critical mass ratio $q_{\text{crit}}^{\text{th}}$ above which mass transfer occurs on the thermal time-scale (Hjellming 1989; Politano 1996):

It is well known that PCEBs that start thermal time-scale mass transfer when the donor first fills its Roche-lobe may still become CVs with AML driven mass transfer as soon as the mass ratio becomes $\lesssim 1$ (Schenker et al. 2002) and if they do not become dynamically unstable first. Such CVs and their progenitors have indeed been observed (Gänsicke et al. 2003b; Parsons et al. 2015) but most likely do not make up more than a few per cent of the entire CV population. The original prescription from Hurley et al. (2002) is known to underestimate the mass transfer rates for thermal time-scale mass transfer. This problem can be fixed to some degree by incorporating an additional factor in the mass transfer equation but the obtained mass transfer can still be off by more than a factor of three (Claeys et al. 2014; Wijnen et al. 2015). For simplicity and because only few CVs are assumed to have evolved through thermal time-scale mass transfer, we kept the original thermal time-scale mass transfer equation in the upgraded version of BSE. The only difference is that the procedure described in Hurley et al. (2002, sections 2.6.3 and 2.6.6) is applied only if the CV is going through thermally unstable mass transfer. Users of the upgraded version of BSE should take into account the potential shortcomings of the treatment of thermal time-scale mass transfer.

A5 Comparison with old prescriptions

In order to illustrate that our modifications lead to CV evolution that is in much better agreement with observations than the old prescriptions, we discuss the evolution of four individual binaries with MS donor masses of 0.13, 0.25, 0.42 and 0.9 M_{\odot} and WD masses of 0.74, 0.73, 0.78 and 1.30 M_{\odot} , respectively. According to the masses of the donor stars, two of them are born above the gap (i.e. long-period CVs) and one each below (i.e. short-period) and in the gap. Figure A1 shows the evolution of these systems in the donor mass vs. period (left-hand panel) plane and mass transfer rate vs. period (right-hand panel) plane. In addition to the predictions of the upgraded and the original BSE code we also show the best-fit model of Knigge et al. (2011).

Figure A1 clearly shows that the period gap cannot be reproduced by the original BSE code (dark violet crosses in Fig. A1). While the mass transfer rate drops when the donor becomes fully convective because AML from MB vanishes (at an orbital period of ≈ 3 hrs), the system born above the gap never detaches because the radius of the donor is assumed not to be affected by mass transfer. The second obvious flaw of the original BSE code are the extremely long periods predicted for period-bouncers which are caused by assuming a non-realistic donor mass-radius relation when the donor becomes degenerate (Section A2). In addition, the mass transfer rate predicted by the original code is not in agreement with the model derived from observations (pink circles in Fig. A1), especially above the gap. This is caused by underestimating the strength of MB, as discussed in Section A3.2.

In contrast, the predictions for CV evolution obtained with the upgraded code (lines in Fig. A1), are in agreement with the observations. The orbital period gap position and width, as well as the location of the period minimum are reproduced correctly. In addition, period-bouncers stay close to the period minimum with small mass transfer rates and the mass transfer rates predicted for CVs above the gap are more realistic.

If fact, let us take as an example the system with WD and donor masses 0.42 and 0.78 M_{\odot} , respectively, which is indicated by the solid red

line. We first note that this system's orbital period decreases due to MB as long as it remains detached (horizontal part of the evolutionary track) and starts its life as a long-period CV at ≈ 3.5 hrs, when mass transfer starts. At this point, the donor is driven out of thermal equilibrium and becomes significantly bloated which causes an increase in the orbital period. When reaching the CV donor mass-radius relation, the orbital period starts to decrease until MB braking becomes inefficient, i.e. when the donor becomes fully convective ($M_d \approx 0.2 M_{\odot}$) at a period of ≈ 3 hrs. At this period, the donor has time to relax to its thermal equilibrium radius and the systems becomes detached. As GR is still acting to remove angular momentum, the orbital period keeps decreasing. This phase of detached evolution corresponds to the orbital period gap (vertical line between 2 and 3 hrs). When the orbital period is ≈ 2 hrs, the Roche lobe has shrunk enough to restart mass transfer and the system becomes a CV again (now as a short-period system). The orbital period is further decreasing until the moment the thermal time-scale exceeds the mass loss time-scale and the donor starts expanding in response to the mass loss. This happens when $M_d \approx 0.07 M_{\odot}$ and $P_{\text{orb}} \approx 1.4$ hrs. From this point on, the CV is a period-bouncer and the donor is degenerate, which causes the period to slightly increase in response to further mass loss and AML.

A6 Final Considerations

We have presented an upgrade of the BSE code that is suitable for performing binary population synthesis of CVs. This upgraded version contains new AML and mass transfer prescriptions. The results we obtain using the upgraded code are in agreement with the standard model of CV evolution and the observations. Some of the prescriptions we incorporated in the new version of BSE are empirical rather than being theoretically well understood. Examples are the strength of magnetic braking which is normalized to reproduce the mass transfer rates of CVs above the period gap, the empirical CAML prescription from Schreiber et al. (2016) which has been invented to explain the absence of low mass WDs among CV primary stars, the mass radius relation for CV donors above the period gap which has been derived from observations (Knigge et al. 2011), and the mass of the donor star at which MB becomes inefficient which has been adjusted to reproduce the width of the orbital period gap (Knigge et al. 2011). Users should be aware of the empirical nature of these prescriptions when using the upgraded BSE code.

Another important fact to be considered is the increased runtime of the upgraded code. The new mass transfer prescription requires smaller timesteps ($\lesssim 10^3$ – 10^4 yrs) which makes the code significantly slower. The original BSE code evolves 1 million binaries in ~ 3 hrs while the upgraded code needs ~ 1 day to evolve the same amount of binaries¹. However, the upgraded code is still the fastest CV evolution code available and is therefore perfectly suitable for population synthesis of CVs. Indeed, we are aware of only one code publicly available that is able to correctly reproduce CV evolution, i.e. the MESA code (e.g. Paxton et al. 2011, 2015; Kalomeni et al. 2016). This stellar evolution code is more accurate than BSE as it does not rely on analytic approximations, but it is also orders of magnitude slower. Other fast publicly available population synthesis codes are SEBA (e.g. Toonen et al. 2012) and BINARY_C (e.g. Izzard et al. 2006). These codes

¹ The simulations presented in this paper were performed on a PSK cluster at the Nicolaus Copernicus Astronomical Centre in Poland.

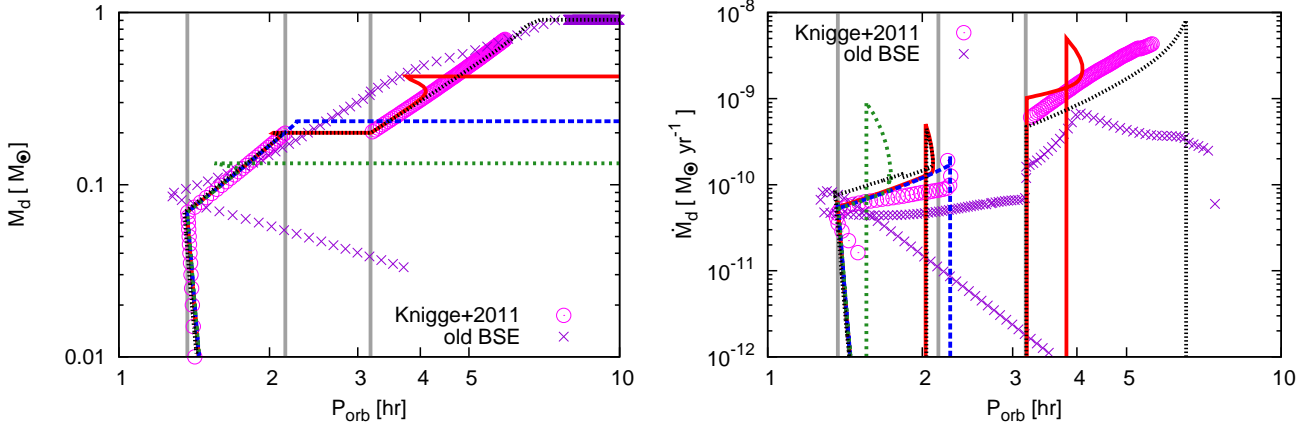


Figure A1. Evolution with orbital period P_{orb} of donor mass M_d (left-hand panel), and mass transfer rate \dot{M}_d (right-hand panel). We show the evolution of four illustrative CVs with initial donor and WD masses: 0.9 and 1.30 M_{\odot} (dotted black line); 0.42 and 0.78 M_{\odot} (solid red line); 0.25 and 0.73 M_{\odot} (dashed blue line); and 0.13 and 0.74 M_{\odot} (short dashed dark green line). We also include in the plots the tracks of the best-fit model by Knigge et al. (2011) (open pink circles) and the tracks of the original BSE code for a CV whose donor mass is 0.9 M_{\odot} (dark violet crosses). For a better comparison with observational constraints, we added to the plots the observational location of the period minimum (Gänsicke et al. 2009) and gap edges (Knigge 2006) (vertical gray lines).

are, however, unable to reproduce CV evolution as described here and give similar results to the old BSE code, i.e. they are similarly not suitable for performing detailed CV population studies (although the upgrades described here can be incorporated into those codes).

In addition to being somewhat slower, CV evolution according to the upgraded version of BSE is limited by assuming a priori solar metallicities. It is still possible to use different metallicities in the input file of the upgraded code (in the same way as in the original code), but the metallicity parameter only affects pre-CV evolution such as the lifetime of the WD progenitor on the MS. As soon as a WD+MS binary starts stable AML driven mass transfer metallicity effects are ignored as we simply use the mass radius relation of Knigge et al. (2011) for the donor star. Fortunately, for population models of CVs metallicity effects are expected to be very small. For example, Stehle et al. (1997) compared CV evolution for solar and sub-solar metallicity and find that low-metallicity CVs produce a slightly smaller period gap, a somewhat shorter minimum period, and in general slightly higher mass transfer rates. This leads to shorter evolutionary time-scales compared to CVs with donors having a solar chemical composition but otherwise the overall evolution is identical. Thus, even though such small differences exist, they should not drastically affect the results of population synthesis, since the objective in such investigations is not to model particular CVs, but rather to establish an overall (statistical) picture for CV evolution.

We would like to draw the readers attention to one important but often overlooked or misinterpreted improvement of the BSE code that was incorporated after the publication of the original BSE paper (Hurley et al. 2002). CEP can now be calculated taking into account recombination energy as described in Claeys et al. (2014, see their Appendix A). The efficiency of recombination energy in contributing to expelling the envelope can be controlled with the parameter λ . A positive value of λ represents the fraction of the recombination energy included in the calculation of the binding energy parameter, $\lambda = 0$ implies that the binding energy parameter is computed assuming recombination energy does not contribute, while for $\lambda < 0$, the binding energy parameter is fixed and set equal to $-\lambda$ (see also Zorotovic et al. 2014).

Finally, all parameters in the code are listed, explained and defined in a file called `parameters.h`. The source code contains an example for population synthesis of CVs and can be downloaded from <http://www.ifa.uv.cl/BSE> or <http://astronomy.swin.edu.au/~jhurley>.

This paper has been typeset from a $\text{\TeX}/\text{\LaTeX}$ file prepared by the author.